CHINESE OPTICS LETTERS

Vol. 22, No. 3 | March 2024

Generation and observation of multiple solitons from a mid-infrared ultrafast fiber laser

Mengyuan Li (李梦媛)[1], Yufeng Song (宋宇锋)[1], Chunxiang Zhang (张春香)[2], Zhenhong Wang (王振洪)[1**], and Jun Liu (刘 军)[1*]

[1] Institute of Microscale Optoelectronics, College of Electronics and Information Engineering, Shenzhen University, Shenzhen 518060, China

[2] Shenzhen Key Laboratory of Ultraintense Laser and Advanced Material Technology, Center for Advanced Material Diagnostic Technology, College of Engineering Physics, Shenzhen Technology University, Shenzhen 518118, China

*Corresponding author: liu-jun-1987@live.cn

**Corresponding author: tjwzh843@163.com

Received October 24, 2023 | Accepted November 9, 2023 | Posted Online March 4, 2024

We demonstrate the generation of a unique regime of multiple solitons in a Tm-doped ultrafast fiber laser at ∼1938.72 nm. The temporal pulse-to-pulse separation among the multiple solitons, 10 in a single-pulse bunch, increases from 0.89 ns to 1.85 ns per round trip. In addition, with the increasing pump power, the number of bunched solitons increases from 3 up to 24 linearly, while the average time separation in the soliton bunch varies irregularly between ∼0.80 and ∼1.52 ns. These results contribute to a more profound comprehension of nonlinear pulse dynamics in ultrafast fiber lasers.

Keywords: mode-locked fiber laser; multiple solitons; pump hysteresis; pulse-to-pulse interval.
DOI: 10.3788/COL202422.031405

1. Introduction

Ultrafast Tm-doped fiber lasers operating in the 1.8–2.1 μm mid-infrared band have attracted considerable attention over the past few decades, owing to their unique operation wavelength band known as the water absorption peak, good eye safety, and transparent atmospheric transmission window[1]. As a result, they have potential benefits for scientific and industrial applications, including medical procedures, plastics processing, lidar, and nanoscale imaging[2–4]. Additionally, they can also serve as an excellent platform for investigating various soliton dynamics, which have attracted much interest in both fundamental physics and nonlinear optics. Generally, the output pulse regime can be determined by the intricate interplay among gain, loss, nonlinearity, and dispersion effects in ultrafast fiber lasers, which are featured as the typical dissipative structures[5,6]. Arising from the peak power limiting effect of the laser cavity[7], high pump intensity-induced nonlinear effects can possibly result in the generation of multiple solitons. The interplay among multiple solitons can give rise to a variety of pulse dynamics based on different mechanisms. Multiple pulse operation is a commonly observed regime, and several interesting phenomena have been reported in the 1 and 1.5 μm bands, including noise-like pulses[8], soliton molecules[9,10], and soliton rain[11]. Bound solitons, known as one typical family member of multiple solitons existing in fiber lasers, were initially proposed in the 1990s in theory based on the nonlinear Schrödinger and complex Ginzburg–Landau equations[12–15]. Basically, multiple solitons can be formed through the interactions among the same type of soliton pulses, including direct local interactions between solitons, long-range interactions mediated by dispersive waves, and continuous wave (CW) mediated global soliton interactions[16]. These kinds of soliton interactions can have different acting ranges and magnitudes of acting forces under specific cavity conditions. It is worth noting that these three kinds of soliton interactions can coexist simultaneously or occur independently, depending on the intracavity parameters. The regular distribution for multiple pulse sequences is also closely related to these interactions among the pulses. The unique characteristics of multiple pulses play a crucial role in various applications. For instance, the long-term stabilization of multiple solitons can be of great significance for optical information storage and transmission[17]. In addition, multiple pulses with appropriate temporal separations and pulse energies can contribute to the mitigation of heat accumulation and thermal damage, making them highly promising for applications in the industrial and medical fields[18,19]. Multiple solitons, under specific tailoring of the pulse separation and phase delay (e.g. large pulse separations and various phase delays), can also experience instable transient behaviors and exhibit intricate pulse dynamics phenomena, such as time jitter[20] and pulsating behavior in loosely bound solitons[21]. These observations have witnessed the complexity and rich dynamics of multiple solitons. Currently, in the 2 μm mid-infrared band, various types of multiple soliton pulses

have been investigated, such as harmonic mode locking[22,23], tightly bound state solitons[24], and bunch state solitons[25]. However, the interactions between multiple pulses can exhibit either weak or strong effects, giving rise to numerous unexplored pulse dynamics. Exploring these pulse dynamics not only enriches the understanding of the nonlinear dissipative laser system with multiple solitons but also facilitates the discovery of intriguing nonlinear optical phenomena.

In this paper, we experimentally observed the generation of multiple solitons in a Tm-doped mode-locked fiber laser based on the nonlinear polarization rotation (NPR) effect. Notably, this is the first systematic exploration of this phenomenon in the 2 μm band, to our best knowledge. As the pump power increases, the total number of pulses in a single multisoliton bunch exhibits a linear increase, while the average temporal separation between pulses within the bunch varies randomly. The temporal separation between pulses in the bunch gradually increases with time. Additionally, the interactions within the multiple solitons are investigated based on numerical simulation, suggesting that the weak acting force can generate interference fringes.

2. Experimental Setup

The schematic diagram of the mode-locked Tm-doped fiber laser is shown in Fig. 1. The laser cavity has a length of 17.3 m, consisting of a 17.1 m single-mode fiber (SMF-28e) and a 0.2 m single-mode thulium-doped fiber (TDF, Nufern, SM-TSF-5/125). In addition, the group velocity dispersion (GVD) coefficients of the SMF and TDF are approximately $\sim -71\ \mathrm{ps}^2/\mathrm{km}$ and $\sim -44.75\ \mathrm{ps}^2/\mathrm{km}$ at 1900 nm, respectively. Consequently, the net cavity dispersion is calculated as $-1.22\ \mathrm{ps}^2$. A polarizer is strategically positioned between the two polarization controllers (PCs), which can form an artificial saturable absorber based on the NPR mechanism. The angles of the PC blades can be adjusted to optimize the polarization state within the cavity. The gain medium is provided by a segment of TDF pumped by a 1570 nm fiber laser through a 1570/2000 nm wavelength division multiplexer (WDM). Unidirectional laser operation is ensured by a polarization-independent isolator (PI-ISO) in the cavity. The laser output is coupled out of the oscillator through a 30/70 optical coupler (OC). The output spectrum and temporal pulse characteristics were measured using an optical spectrum analyzer (OSA, Yokogawa, AQ6375B) and an oscilloscope (Tekrtonix, DPO71254C) with a photodetector (EOT-5000), respectively. The radio-frequency (RF) spectrum is recorded by an RF analyzer (Keysight, N9322C). The pulse duration was measured by a commercial autocorrelator (APE-150 Pulsecheck).

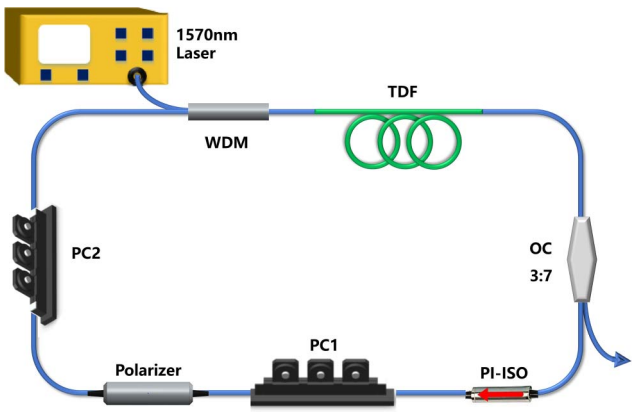

Fig. 1. Schematic diagram of the experiment setup.

3. Experimental Results and Discussions

With an increase in the pump power and appropriate adjustment of the PCs' paddles, stable mode-locking operation can be realized. Specifically, at a pump power of 665 mW, the laser can be operated in a single-pulse regime by appropriately changing the PCs. Figure 2(a) presents the corresponding spectrum,

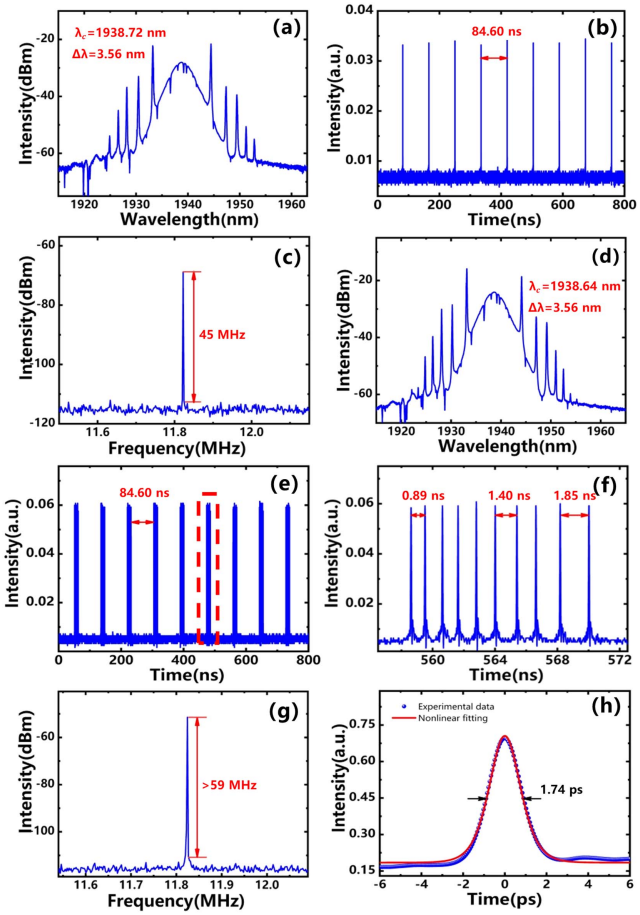

Fig. 2. Mode-locking operation of single and multiple solitons at different pump powers. Single soliton at 665 mW: (a) optical spectrum, (b) temporal pulse train, and (c) RF spectrum. Multiple solitons at 925 mW: (d) optical spectrum, (e) temporal pulse trains, (f) close-up of the temporal pulse trains for multiple solitons in (e), (g) RF spectrum with a 1 MHz span, and (h) autocorrelation trace.

centered at 1938.72 nm, with a 3-dB bandwidth of 3.56 nm. We can see that the Kelly sidebands on the spectrum are not symmetric across the main peak. This is attributed to the spectral interference of dispersive waves. Notably, there are some dips in the spectrum, which corresponds to the water absorption peaks in the 2 μm band. The mode-locking pulse train is depicted in Fig. 2(b). The temporal period (i.e., the time period between adjacent pulses) is 84.6 ns, corresponding to a fundamental frequency of 11.82 MHz, which is determined by the cavity length of ~17.3 m. The RF spectrum is presented in Fig. 2(c), illustrating a signal-to-noise ratio (SNR) of 45 dB at the frequency peak of 11.82 MHz. With a slight adjustment of the PCs, when the pump power is increased beyond 725 mW, the laser switches from the single-pulse regime to the multiple-pulse state. Figure 2(d) shows the spectrum of the soliton bunch at a pump power of 825 mW. The center wavelength is 1938.64 nm and similar Kelly sidebands are observed as the previous ones [see Fig. 2(a)]. The corresponding pulse trains are displayed in Figs. 2(e) and 2(f). It can be seen that the laser is operating in the multiple-pulse bunch state, with a temporal interval between adjacent pulse bunches of 84.60 ns. Figure 2(f) provides a detailed zoom-in view within the red dashed area in Fig. 2(e). Clearly, there are 10 soliton pulses within a single multiple-pulse bunch, illustrating the typical multipulse operation regime. The pulse-to-pulse separation within the bunch ranges from ~0.89 to 1.85 ns. The RF spectrum in Fig. 2(h) exhibits a high SNR of more than 59 dB at the fundamental frequency of 11.82 MHz, which indicates the steady operation state of multiple pulses. The autocorrelation curve, shown in Fig. 2(g), is well fitted to a sech^2 pulse profile. The pulse duration is measured to ~1.12 ps, with a full width at half-maximum (FWHM) value of 1.74 ps.

The temporal characteristics of the soliton bunches are further evaluated by the three-dimensional (3D) spatiotemporal evolution diagram. Figure 3 shows the multiple-pulse bunches' 3D spatiotemporal evolution over 3600 round trips at different pump powers. We can see from Fig. 3(a) that the multiple-pulse bunch consists of 13 soliton pulses at a pump power of 1025 mW. The temporal separations between adjacent pulses vary from 0.66 to 1.53 ns, with an approximate average separation of 0.94 ns. When increasing the pump power up to 1225 mW without changing the PCs, we observe a notable increase in the number of pulses within a multiple-pulse bunch, as depicted in Fig. 3(b). The single multiple-pulse bunch has 18 pulses. And the interpulse temporal separation ranges from 0.66 to 1.46 ns, with a calculated average separation of ~0.80 ns. In addition, it is evident that, over a single cavity round trip, the interpulse temporal separations under the two different pump powers both increase gradually with time, as shown in Figs. 3(a) and 3(b), underlining the weak long-distance interactions within the multiple pulses. This can be attributed to the characteristic variation in the interpulse temporal separation resulting from the gain modulation caused by gain-absorption depletion and recovery effects[26]. Moreover, with the increase of pump power, a larger nonlinearity is introduced and accumulated in the laser cavity, which can ultimately result in an increase in the number of pulses in the resonant cavity owing

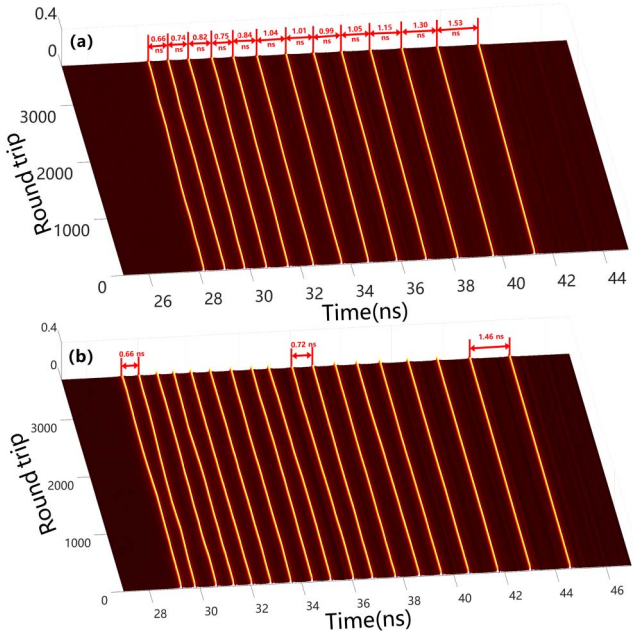

Fig. 3. Spatiotemporal evolution diagrams of multiple solitons at different pump powers. (a) 1025 mW, (b) 1225 mW.

to the peak-power-clamping effect and excessive pulse chirp in the resonator[7]. The variation in the number of multiple pulses across a single round trip with pump power is illustrated in Fig. 4(a). It is evident that the bunch exhibits a linear increase in the number of pulses, ranging from 3 to 24, as the pump power increases. Furthermore, we calculate the average interpulse separation in a multiple-pulse bunch, as shown in Fig. 4(b). The average separation changes irregularly when increasing the pump power, which is different from previous reports[20,21,27], where a decrease in the average interpulse separation was found with the pump power. This indicates that the direct pulse-to-pulse interaction among the bunch frequently changes, depending on the cavity conditions (e.g., the exact pump power)[20,21,27]. We can see from Figs. 3(a) and 3(b) that all these temporal separations between adjacent pulses exceed 0.66 ns, which is much larger than the single-pulse width shown in Fig. 2(g) and cannot be measured by commercially available autocorrelators. Therefore, the multiple pulses obtained in this experiment can be considered as a special class of soliton families. In this situation, the direct pulse-to-pulse interactions within the soliton bunch are weakened as the corresponding temporal separations increase. With a relatively large separation among the multiple solitons, the direct pulse-to-pulse interaction is too weak to play a significant role. In contrast, the long-range interactions mediated by resonant dispersive waves can play an important part in the soliton dynamics and can contribute to the formation of quasi-bound states of solitons as well as the identification of their exact temporal occurrence[28]. The strength of dispersive waves in a fiber laser can be determined by the pump power or the intracavity phase delay bias[16]. It is worth noting that the multiple solitons in this operation state are weakly bounded and less stable. The complex interactions

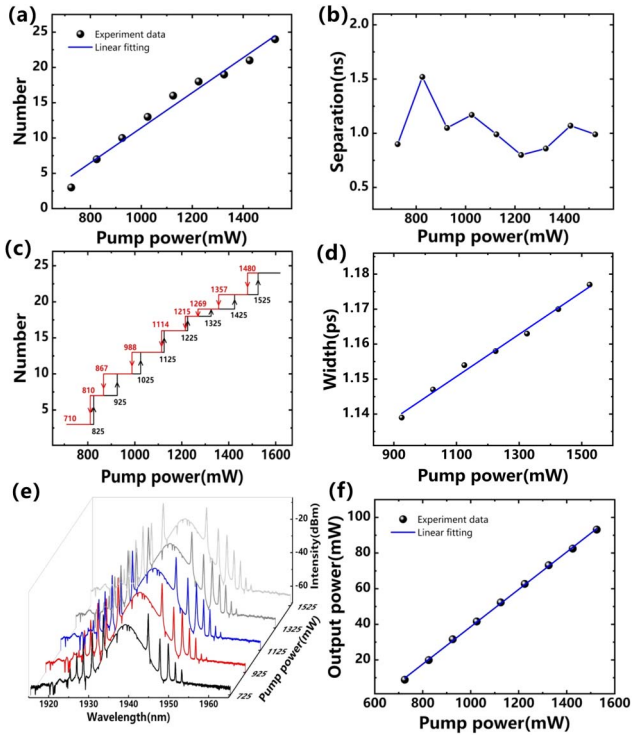

Fig. 4. Soliton bunch characteristics under varying pump powers. (a) Pulse number in single round trip versus pump power; (b) average pulse separation in single round trip versus pump power; (c) pulse number's dependency on the pump power; (d) average pulse width within a soliton bunch versus pump power; (e) optical spectra; and (f) average output power's dependency on pump power.

among the multiple solitons can further determine the relative temporal positions for individual solitons. Thus, the average pulse separation represents an irregular relationship with the pump power. Furthermore, an investigation is also conducted to examine the relationship between the pump power and the total pulse number in the soliton bunch, as shown in Fig. 4(c). The descending and ascending curves are illustrated by the red and black steps, respectively. It can be seen that the number of pulses within the soliton bunch increases from 21 to 24, corresponding to the pump power varying from 1425 to 1525 mW. Besides, the number of pulses in the soliton bunch can be reduced to 21 again when gradually decreasing the pump power to 1480 mW. This exhibits a clear hysteresis phenomenon[29]. Additionally, considering the large interpulse separation among the multiple solitons exceeding the temporal window that can be detected by the commercial autocorrelators, we measure the average pulse width within the multiple-soliton bunch at different pump powers, as depicted in Fig. 4(d). It is evident that the average pulse width of the soliton bunch exhibits a gradual increase with the pump power, indicating a concomitant growth in the total number of pulses within the bunch.

The optical spectrum of the multiple pulses is also evaluated at different pump powers, as shown in Fig. 4(e). Obviously, the output spectra exhibit similar profiles but with slightly different center wavelengths and Kelly sidebands. It is worth noting that all these Kelly sidebands have similar asymmetries, which is closely associated with dispersive wave emissions. These dispersive waves can play a significant role in triggering long-range soliton interactions[7] and thus the formation of multiple solitons. Moreover, it is noteworthy that the spectra exhibit no apparent interference patterns, despite the laser operating in the multiple pulse mode. This can be ascribed to the considerable pulse separations within the soliton bunch, which distinguish it from the closely spaced soliton bundles observed in previous studies[20,27]. Further analysis of the interactions within the multiple solitons will be presented in the subsequent section dedicated to numerical simulations. In addition, we also evaluate the average output powers of multiple pulses at different pump powers. The corresponding results are illustrated in Fig. 4(f), demonstrating an approximately linear increasing trend. The slope efficiency is about 10.78%, and the output power reaches ~93 mW at the maximum pump power of 1525 mW.

In order to further investigate the interaction of multiple solitons within a single-soliton bunch, we conducted numerical analysis concerning the operation of the pulse stretching for a multiple-soliton bunch. This process is based on the analogy between spatial Fraunhofer diffraction and temporal dispersion. When a pulse propagates through a largely dispersive medium, it will be temporally stretched due to the dispersive effect within the medium. Assuming that the dispersion value of the medium is sufficiently large, solitons can be stretched toward their neighbors. This process delves into the subtle but complex interactions between pulses, which may lead to intriguing outcomes. In the simulation, assuming that the superposition of solitons can be used to describe the complex envelope of the multipulse bunch, which slowly varies,

$$u(0,t)=\sum_{k=1}^{N}u_k(t-\tau_k)e^{-i\varphi_k}, \tag{1}$$

where u is the field amplitude of the optical pulse, N is the number of multiple solitons, u_k represents the slowly varying envelope of a single soliton, while the τ_k and φ_k denote the relative position and relative phase of a single soliton. The envelope of the multisoliton pulse after dispersive propagation can be given by[30]

$$|u(L,T)|^2 \propto \left|\sum_{k=1}^{N}\widetilde{u}_k\left(\frac{T-\tau_k}{\beta_2 L}\right)e^{-i\varphi_k}\right|^2, \tag{2}$$

where L is the GVD length, β_2 is the second-order dispersion coefficient, and T is the time in the reference frame of the pulse. This transform establishes a proportional relationship between the temporal and frequency domain characteristics of the optical pulse. By employing the above approach, we can investigate the internal dynamics of multiple pulses, providing a deeper understanding of the interactions among multiple solitons. In this simulation, for better matching of the experimental results, we assume a multisoliton bunch consisting of 13 solitons with adjacent time intervals between the pulses, similar to those

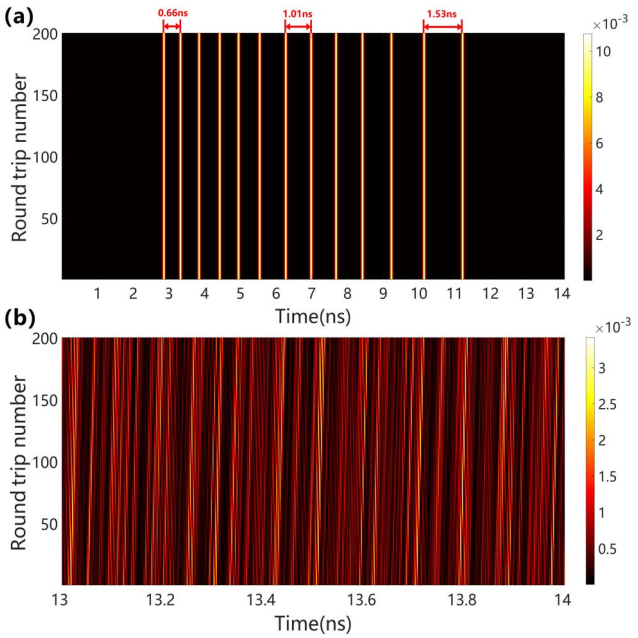

Fig. 5. (a) Numerical simulation of multiple solitons; (b) spatial-temporal diagram at the 13-soliton state.

depicted in Fig. 3(a). The soliton bunch is transmitted over 200 round trips, and the corresponding spatiotemporal diagram is depicted in Fig. 5(a). Additionally, the spatiotemporal diagram achieved after propagating through a largely dispersive medium is shown in Fig. 5(b). Notably, clear interference patterns are observed, indicating the existence of complex interactions among adjacent pulses. This may potentially provide novel perspectives and understandings for the research of multisolitons in the 2 μm band.

4. Conclusion

In conclusion, we report the observation of multiple solitons with unique features in a mid-infrared ultrafast fiber laser, for the first time to our knowledge. Characteristics of the multiple pulses within a single-soliton bunch in terms of the temporal separations between pulses and the number of subpulses can be influenced by the gain-absorption depletion and recovery effect in the laser system. The total number of pulses within one single-soliton bunch exhibits a linear increase with the pump power. Moreover, the interpulse separation between adjacent pulses within the soliton bunch gradually increases across a single round trip, ranging from hundreds of picoseconds to a few nanoseconds. However, the average pulse separation fluctuates irregularly with increasing pump power. Finally, we conduct a numerical analysis to examine the interactions among multiple pulses at different interpulse separations. It is believed that the presented results can contribute significantly to advancing the comprehension of nonlinear soliton dynamics in the 2 μm wavelength band.

Acknowledgements

This work was supported by the National Natural Science Foundation of China (Nos. 61935013, 61975133, and 62005178), the Guangdong Major Project of Basic and Applied Basic Research (No. 2020B0301030009), the Natural Science Foundation of Guangdong Province (No. 2023A1515010093), the Science and Technology Innovation Commission of Shenzhen, Shenzhen Peacock Plan (Nos. KQTD20170330110444030, JCYJ20200109114018750, and JCYJ20220809170611004), and Shenzhen University (No. 2019075).

References

1. C. W. Rudy, M. J. F. Digonnet, and R. L. Byer, "Advances in 2-μm Tm-doped mode-locked fiber lasers," Opt. Fiber Technol. **20**, 642 (2014).
2. I. T. Sorokina, V. V. Dvoyrin, N. Tolstik, *et al.*, "Mid-IR ultrashort pulsed fiber-based lasers," IEEE J. Sel. Top. Quantum Electron. **20**, 99 (2014).
3. K. Yin, B. Zhang, G. Xue, *et al.*, "High-power all-fiber wavelength-tunable thulium doped fiber laser at 2 μm," Opt. Express **22**, 19947 (2014).
4. N. M. Fried and K. E. Murray, "High-power thulium fiber laser ablation of urinary tissues at 1.94 μm," J. Endourol. **19**, 25 (2005).
5. F. Ö. Ilday, J. R. Buckley, W. G. Clark, *et al.*, "Self-similar evolution of parabolic pulses in a laser," Phys. Rev. Lett. **92**, 213902 (2004).
6. P. Grelu and N. Akhmediev, "Dissipative solitons for mode-locked lasers," Nat. Photonics **6**, 84 (2012).
7. D. Y. Tang, L. M. Zhao, B. Zhao, *et al.*, "Mechanism of multisoliton formation and soliton energy quantization in passively mode-locked fiber lasers," Phys. Rev. A **72**, 043816 (2005).
8. X. Wang, A. Komarov, M. Klimczak, *et al.*, "Generation of noise-like pulses with 203 nm 3-dB bandwidth," Opt. Express **27**, 24147 (2019).
9. T. Guo, Z. Wang, F. Gao, *et al.*, "Observation of complex multimode soliton molecules in spatiotemporal mode-locked Er-doped fiber laser," Opt. Commun. **524**, 128773 (2022).
10. C. R. Santosh, R. Gowrishankar, and S. Srivastava, "Harmonic mode-locked noise-like pulses under a *Q*-switched envelope in an erbium doped all-fiber ring laser," Appl. Opt. **61**, 7354 (2022).
11. G. W. Chen, K. L. Jia, S. K. Ji, *et al.*, "Soliton rains with isolated solitons induced by acoustic waves in a nonlinear multimodal interference-based fiber laser," Laser Phys. **33**, 035101 (2023).
12. B. A. Malomed, "Bound solitons in the nonlinear Schrödinger–Ginzburg–Landau equation," Phys. Rev. A **44**, 6954 (1991).
13. B. A. Malomed, "Bound solitons in coupled nonlinear Schrödinger equations," Phys. Rev. A **45**, R8321 (1992).
14. N. Akhmediev, A. Ankiewicz, and J. Soto-Crespo, "Multisoliton solutions of the complex Ginzburg-Landau equation," Phys. Rev. Lett. **79**, 4047 (1997).
15. N. N. Akhmediev, A. Ankiewicz, and J. M. Soto-Crespo, "Stable soliton pairs in optical transmission lines and fiber lasers," J. Opt. Soc. Am. B **15**, 515 (1998).
16. D. Y. Tang, B. Zhao, L. M. Zhao, *et al.*, "Soliton interaction in a fiber ring laser," Phys. Rev. E **72**, 016616 (2005).
17. W. He, M. Pang, D. H. Yeh, *et al.*, "Formation of optical supramolecular structures in a fibre laser by tailoring long-range soliton interactions," Nat. Commun. **10**, 5756 (2019).
18. C. Kerse, H. Kalaycıoğlu, P. Elahi, *et al.*, "Ablation-cooled material removal with ultrafast bursts of pulses," Nature **537**, 84 (2016).
19. R. R. Gattass, L. R. Cerami, and E. Mazur, "Micromachining of bulk glass with bursts of femtosecond laser pulses at variable repetition rates," Opt. Express **14**, 5279 (2006).
20. Z. Wang, Z. Wang, Y. Liu, *et al.*, "Generation and time jitter of the loose soliton bunch in a passively mode-locked fiber laser," Chin. Opt. Lett. **15**, 080605 (2017).

21. Z. Wang, X. Wang, Y. Song, *et al.*, "Generation and pulsating behaviors of loosely bound solitons in a passively mode-locked fiber laser," Phys. Rev. A **101**, 013825 (2020).
22. Y. Wang, J. Li, E. Zhang, *et al.*, "Coexistence of noise-like pulse and high repetition rate harmonic mode-locking in a dual-wavelength mode-locked Tm-doped fiber laser," Opt. Express **25**, 17192 (2017).
23. K. Yin, B. Zhang, L. Li, *et al.*, "Soliton mode-locked fiber laser based on topological insulator Bi_2Te_3 nanosheets at 2 μm," Photonics Res. **3**, 72 (2015).
24. X. Ren, H. Li, Z. Zhang, *et al.*, "Generation of bound solitons in a mode-locked Tm-doped fiber laser based on a graded-index multimode fiber saturable absorber," Opt. Laser Technol. **149**, 107865 (2022).
25. P. Hu, J. Mao, X. Zhou, *et al.*, "Multiple soliton mode-locking operations of a Holmium-doped fiber laser based on nonlinear polarization rotation," Opt. Laser Technol. **161**, 109218 (2023).
26. A. Zaviyalov, P. Grelu, and F. Lederer, "Impact of slow gain dynamics on soliton molecules in mode-locked fiber lasers," Opt. Lett. **37**, 175 (2012).
27. Z. Wang, C. Ma, Y. Song, *et al.*, "Simultaneous generation and real-time observation of loosely bound solitons and noise-like pulses in a dispersion-managed fiber laser with net-normal dispersion," Opt. Express **28**, 39463 (2020).
28. L. Socci and M. Romagnoli, "Long-range soliton interactions in periodically amplified fiber links," J. Opt. Soc. Am. B **16**, 12 (1999).
29. A. Komarov, H. Leblond, and F. Sanchez, "Multistability and hysteresis phenomena in passively mode-locked fiber lasers," Phys. Rev. A **71**, 053809 (2005).
30. K. Goda and B. Jalali, "Dispersive Fourier transformation for fast continuous single-shot measurements," Nat. Photonics **7**, 102 (2013).